Available online at www.sciencedirect.com
SCIENCE DIRECT®
ELSEVIER
Experimental Thermal and Fluid Science xxx (2004) xxx–xxx
Experimental Thermal and Fluid Science
www.elsevier.com/locate/etfs

# Experiment of falling cylinder through the water column

Peter C. Chu *, Anthony Gilles, Chenwu Fan

*Naval Ocean Analysis and Prediction Laboratory, Department of Oceanography, Naval Postgraduate School, Monterey, CA 93943, United States*

Received 28 January 2004; accepted 12 August 2004

**Abstract**

Hydrodynamic features of a falling cylinder into the water column are investigated experimentally. The experiment consisted of dropping three cylinders of various lengths into a pool where the trajectories were filmed from two angles. The controlled parameters are cylinder's physical parameters (length to diameter ratio, center of mass location), and initial drop conditions (initial velocity, and drop angle). Six trajectory patterns (straight, spiral, flip, flat, seesaw, combination) are detected during the experiment. The center of mass position has the largest influence on the trajectory of cylinders. The observed motion of cylinders is well simulated using a numerical model based on the momentum and moment of momentum balances using triple coordinate transform.


*Keywords:* Cylinder; Cylinder drop experiment; Center of mass; Center of volume; Trajectory pattern



## 1. Introduction

Study on the movement of a rigid body in fluid has wide scientific significance and technical application. It involves nonlinear dynamics, flight theory, body–fluid interaction, and instability theory (e.g., [1]). The technical application of fluid mechanics of a rigid body in fluid includes aeronautics and navigation. Recently, the scientific problem about rigid body movement in the water column drew attention to the naval research. This is due to the threat of mines in the naval operations. Within the past 15 years three US ships, the USS Samuel B. Roberts (FFG-58), Tripoli (LPH-10) and Princeton (CG-59) have fallen victim to mines. Total ship damage was $125 million while the mines cost approximately $30 thousand [2]. Mines have evolved over the years from the dumb "horned" contact mines that damaged the Tripoli and Roberts to ones that are relatively sophisticated—non-magnetic materials, irregular shapes, anechoic coatings, multiple sensors and ship count routines. Despite their increased sophistication, mines remain inexpensive and are relatively easy to manufacture, keep and place. Water mines are characterized by three factors: position in water (bottom, moored, rising, and floating), method of delivery (aircraft, surface, subsurface) and method of actuation (acoustic and/or magnetic influence, pressure, contact, controlled).

Prediction of a falling rigid body in the water column is a key component in determining the impact speed and direction of mine on the sediment and in turn in determining its burial depth and orientation. In this study, a cylinder drop experiment was conducted to investigate dynamical characteristics of the falling cylinder through the water column.

## 2. Triple coordinate systems

Consider an axially symmetric cylinder with the center of mass (COM) **X** and center of volume (COV) **B** on the main axis (Fig. 1). Let $(L, d, \chi)$ represent the cylinder's length, diameter, and the distance between the

* Corresponding author. Tel.: +1 831 656 3688; fax: +1 831 656 3686.
*E-mail address:* chu@nps.navy.mil (P.C. Chu).

0894-1777/$ - see front matter © 2004 Published by Elsevier Inc.
doi:10.1016/j.expthermflusci.2004.08.001

## Nomenclature

| | |
|---|---|
| ($C_{d1}$, $C_{d2}$) | drag coefficients along and across the cylinder |
| ($C_{td1}$, $C_{td2}$) | translational drag coefficients ($\mathrm{kg\,s^{-1}}$) |
| $C_l$ | lift coefficient |
| $C_{tl}$ | translational lift coefficient ($\mathrm{kg\,s^{-1}}$) |
| $d$ | cylinder diameter (m) |
| ($f_1$, $f_2$, $f_3$) | added-mass ratios for drag and lift forces |
| $f_r$ | added-mass ratio for moment of drag and lift forces |
| ($f_{rd2}$,$f_{rd3}$) | rotational drag force (N) |
| $\mathbf{F}_b$ | buoyancy force (N) |
| $\mathbf{F}_d$ | drag force (N) |
| ($\mathbf{F}_{d1}$, $\mathbf{F}_{d2}$, $\mathbf{F}_{d3}$) | drag force in the $F$-coordinate (N) |
| $\mathbf{F}_l$ | lift force (N) |
| ($\mathbf{F}_{l1}$, $\mathbf{F}_{l2}$, $\mathbf{F}_{l3}$) | lift force in the $F$-coordinate (N) |
| ($\mathbf{i}_E$, $\mathbf{j}_E$, $\mathbf{k}_E$) | unit vectors in the $E$-coordinate |
| ($\mathbf{i}_F$, $\mathbf{j}_F$, $\mathbf{k}_F$) | unit vectors in the $F$-coordinate |
| ($\mathbf{i}_M$, $\mathbf{j}_M$, $\mathbf{k}_M$) | unit vectors in the $M$-coordinate |
| ($J_1$, $J_2$, $J_3$) | moments of gyration ($\mathrm{kg\,m^2}$) |
| ($J_1^{(i)}$, $J_2^{(i)}$, $J_3^{(i)}$) | moments of gyration for cylindrical part-$i$ ($\mathrm{kg\,m^2}$) |
| $L$ | length of the cylinder (m) |
| ($l_1$, $l_2$, $l_3$) | lengths of the cylindrical parts (m) |
| ($m_1, \ldots, m_6$) | masses of cylindrical parts (kg) |
| $\mathbf{M}_b$ | torque due to the buoyancy force ($\mathrm{kg\,m^2\ s^{-2}}$) |
| $\mathbf{M}_h$ | torque due to the hydrodynamic force ($\mathrm{kg\,m^2\ s^{-2}}$) |
| ($\mathbf{M}_{d1}$, $\mathbf{M}_{d2}$, $\mathbf{M}_{d3}$) | torques due to the drag force in the $M$-coordinate ($\mathrm{kg\,m^2\,s^{-2}}$) |
| ($R_1$, $R_2$, $R_3$) | radii of cylindrical parts (m) |
| $Re$ | Reynolds number |
| $\mathbf{V}$ | translation velocity ($\mathrm{m\,s^{-1}}$) |
| $\mathbf{V}_r$ | water-to-cylinder velocity ($\mathrm{m\,s^{-1}}$) |
| $\mathbf{V}_1$ | component of $\mathbf{V}_r$ along the cylinder ($\mathrm{m\,s^{-1}}$) |
| $\mathbf{V}_2$ | component of $\mathbf{V}_r$ perpendicular to the cylinder ($\mathrm{m\,s^{-1}}$) |
| $\mathbf{V}_w$ | water velocity ($\mathrm{m\,s^{-1}}$) |
| $\mathbf{V}^{(in)}$ | initial speed of dropping cylinder ($\mathrm{m\,s^{-1}}$) |
| $\mathbf{V}^*$ | nondimensional translation velocity |
| ($\alpha_0, \ldots, \alpha_4$) | correlation coefficients for predicting bottom impact velocity and orientation |
| $[\beta_0(t), \ldots, \beta_4(t)]$ | correlation coefficients for predicting translation velocity and orientation of the falling cylinders |
| $\delta$ | aspect ratio of the cylinder |
| $\lambda$ | distance between adjustable copper cylindrical part (m) |
| $v$ | molecular viscosity of the water ($\mathrm{m^2\,s^{-1}}$) |
| $\Pi$ | volume of the cylinder ($\mathrm{m^3}$) |
| $\rho$ | density of the cylinder ($\mathrm{kg\,m^{-3}}$) |
| $\rho_w$ | density of the water ($\mathrm{kg\,m^{-3}}$) |
| $\chi$ | distance between COM and COV (m) |
| ($\psi_1$, $\psi_2$, $\psi_3$) | angles determining the cylinders' orientation |
| $\boldsymbol{\omega}$ | angular velocity ($\mathrm{s^{-1}}$) |
| ($\omega_1$, $\omega_2$, $\omega_3$) | angular velocity components in the $M$-coordinate ($\mathrm{s^{-1}}$) |
| ($\omega_1', \omega_2', \omega_3'$) | angular velocity components in the $F$-coordinate ($\mathrm{s^{-1}}$) |

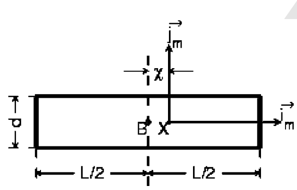

Fig. 1. $M$-coordinate with the COM as the origin $X$ and ($i_m$, $j_m$) as the two axes. Here, $\chi$ is the distance between the COV($B$) and COM ($L,d$) are the cylinder's length and diameter.

two points ($\mathbf{X}, \mathbf{B}$). The positive $\chi$-values refer to nose-down case, i.e., the point $\mathbf{X}$ is lower than the point $\mathbf{B}$. Three coordinate systems are used to model the falling cylinder through the air, water, and sediment phases: earth-fixed coordinate ($E$-coordinate), main-axis following coordinate ($M$-coordinate), and force following coordinate ($F$-coordinate) systems. All the systems are three-dimensional, orthogonal, and right-handed. The origin of $M$- and $F$-coordinates is located at $\mathbf{X}$ [3].

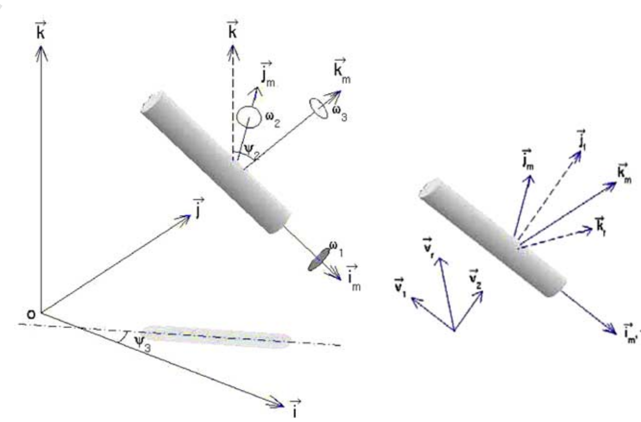

Fig. 2. Three coordinate systems.

The $E$-coordinate is represented by $F_E$ ($O$, $\mathbf{i}$, $\mathbf{j}$, $\mathbf{k}$) with the origin '$O$', and three axes: $x$-, $y$-axis (horizontal) with the unit vectors ($\mathbf{i}, \mathbf{j}$) and $z$-axis (vertical) with the unit vector $k$ (upward positive) (see Fig. 2). The position of the cylinder is represented by the COM position

$$\mathbf{X} = x\mathbf{i} + y\mathbf{j} + z\mathbf{k}. \tag{1}$$

The translation velocity is given by

$$\frac{\mathrm{d}\mathbf{X}}{\mathrm{d}t} = \mathbf{V}, \mathbf{V} = (u, v, w). \tag{2}$$

The orientation of the cylinder's main-axis (pointing downward) is given by $\mathbf{i}_M$. The angle between $\mathbf{i}_M$ and $\mathbf{k}$ is denoted by $\psi_2 + \pi/2$. Projection of the vector $\mathbf{i}_M$ onto the $(x, y)$ plane creates angle $(\psi_3)$ between the projection and the $x$-axis (Fig. 2). The $M$-coordinate is represented by $\mathbf{F}_M$ $(\mathbf{X}, \mathbf{i}_M, \mathbf{j}_M, \mathbf{k}_M)$ with the origin '$\mathbf{X}$', unit vectors $(\mathbf{i}_M, \mathbf{j}_M, \mathbf{k}_M)$, and coordinates $(x_M, y_M, z_M)$. The unit vectors of the $M$-coordinate system are given by (Fig. 2)

$$\mathbf{j}_M = \mathbf{k} \times \mathbf{i}_M, \quad \mathbf{k}_M = \mathbf{i}_M \times \mathbf{j}_M \tag{3}$$

The $M$-coordinate system is solely determined by the orientation of the cylinder's main-axis $\mathbf{i}_M$.

The $F$-coordinate is represented by $F_F$ $(\mathbf{X}, \mathbf{i}_F, \mathbf{j}_F, \mathbf{k}_F)$ with the origin $\mathbf{X}$, unit vectors $(\mathbf{i}_F, \mathbf{j}_F, \mathbf{k}_F)$, and coordinates $(x_F, y_F, z_F)$. Let $\mathbf{V}_\mathrm{w}$ be the fluid velocity. The water-to-cylinder velocity is represented by

$$\mathbf{V}_\mathrm{r} = \mathbf{V}_\mathrm{w} - \mathbf{V}, \tag{4}$$

which can be decomposed into two parts,

$$\begin{aligned} &\mathbf{V}_\mathrm{r} = \mathbf{V}_1 + \mathbf{V}_2, \quad \mathbf{V}_1 = (\mathbf{V}_\mathrm{r} \cdot \mathbf{i}_F)\mathbf{i}_F, \\ &\mathbf{V}_2 = \mathbf{V}_\mathrm{r} - (\mathbf{V}_\mathrm{r} \cdot \mathbf{i}_F)\mathbf{i}_F, \end{aligned} \tag{5}$$

where $\mathbf{V}_1$ is the component parallel to the cylinder's main-axis (i.e., along $\mathbf{i}_M$), and $\mathbf{V}_2$ is the component perpendicular to the cylinder's main-axial direction. The unit vectors for the $F$-coordinate are defined by (column vectors)

$$\mathbf{i}_F = \mathbf{i}_M, \quad \mathbf{j}_F = \mathbf{V}_2/|\mathbf{V}_2|, \quad \mathbf{k}_F = \mathbf{i}_F \times \mathbf{j}_F. \tag{6}$$

In the $F$-coordinate, the hydrodynamic forces (drag, lift) and torques are easily computed [4–6].

## 3. Dynamics

### 3.1. Momentum balance

The translation velocity of the cylinder ($\mathbf{V}$) is governed by the momentum equation in the $E$-coordinate system [1]

$$\frac{\mathrm{d}}{\mathrm{d}t}\begin{bmatrix} u \\ v \\ w \end{bmatrix} = -\begin{bmatrix} 0 \\ 0 \\ g \end{bmatrix} + \frac{\mathbf{F}_\mathrm{b} + \mathbf{F}_\mathrm{h}}{\rho \Pi}, \tag{7}$$

where $g$ is the gravitational acceleration; $\Pi$ is the cylinder volume; $\rho$ is the rigid body density; $\rho\Pi = m$, is the cylinder mass; $\mathbf{F}_\mathrm{h}$ is the hydrodynamic force (i.e., surface force including drag, lift, impact forces); $\mathbf{F}_\mathrm{b} = -\rho_\mathrm{w}\Pi$, is the buoyancy force; and $\rho_\mathrm{w}$ is the water density. The drag and lift forces are calculated using the drag and lift laws with the given water-to-cylinder velocity ($\mathbf{V}_\mathrm{r}$). In the $F$-coordinate, $\mathbf{V}_\mathrm{r}$ is decomposed into along-cylinder ($\mathbf{V}_1$) and across-cylinder ($\mathbf{V}_2$) components.

### 3.2. Moment of momentum equation

It is convenient to write the moment of momentum equation [1]

$$\mathbf{J} \cdot \frac{\mathrm{d}\boldsymbol{\omega}}{\mathrm{d}t} = \mathbf{M}_\mathrm{b} + \mathbf{M}_\mathrm{h}, \tag{8}$$

in the $M$-coordinate system with the cylinder's angular velocity components $(\omega_1, \omega_2, \omega_3)$ defined by (4). Here, $\mathbf{M}_\mathrm{b}$ and $\mathbf{M}_\mathrm{h}$ are the buoyancy and hydrodynamic force torques. The buoyancy force induces the moment in the $\mathbf{j}_M$ direction if the COM does not coincide with the COV (i.e., $\chi \neq 0$),

$$\mathbf{M}_\mathrm{b} = \Pi\chi\rho_\mathrm{w} g \cos\psi_2 \mathbf{j}_M. \tag{9}$$

In the $M$-coordinate system, the tensor $\mathbf{J}$ for the axially symmetric cylinder is represented by a diagonal matrix

$$\mathbf{J} = \begin{bmatrix} J_1 & 0 & 0 \\ 0 & J_2 & 0 \\ 0 & 0 & J_3 \end{bmatrix}, \tag{10}$$

where $J_1$, $J_2$, and $J_3$ are the moments of gyration about the center of mass. The gravity force, passing the center of mass, does not induce the moment.

## 4. Hydrodynamic force and torque

The hydrodynamic force ($\mathbf{F}_\mathrm{h}$) and torque ($\mathbf{M}_\mathrm{h}$) are easily calculated in the $F$-coordinate system using existing formulas. After calculation, the hydrodynamic force ($\mathbf{F}_\mathrm{h}$) should be transformed from the $F$-coordinate to the $E$-coordinate before substituting into the momentum Eq. (7), and the hydrodynamic torque ($\mathbf{M}_\mathrm{h}$) should be transformed from the $F$-coordinate to the $M$-coordinate before substituting into the moment of momentum equation (8) for solutions [3].

### 4.1. Drag force

The drag force consists of three parts: (a) along $\mathbf{i}_F$ (along-cylinder) drag-force ($\mathbf{F}_{\mathrm{d}1}$), (b) along $\mathbf{j}_F$ (across-cylinder) drag force ($\mathbf{F}_{\mathrm{d}2}$), and (3) along $\mathbf{k}_F$ drag force ($\mathbf{F}_{\mathrm{d}3}$). Let $(C_{\mathrm{d}1}, C_{\mathrm{d}2})$ be the drag coefficients along- and across-cylinder directions (Reynolds number dependent). The drag force coefficients are calculated on the base of steady flow, it is different from the fluid around an accelerated solid body. The added mass correction is represented by the ratios ($f_1$,$f_2$,$f_3$) in the three directions of the $F$-coordinate system.

The drag force along-$\mathbf{i}_F$ is calculated by

$$\mathbf{F}_{\mathrm{d}1} = \mathbf{i}_F C_{f1} V_1, \quad C_{f1} \equiv C_{\mathrm{d}1} \frac{\pi d^2}{8} \frac{\rho_{\mathrm{w}}}{(1+f_1)} |\mathbf{V}_1|, \tag{11}$$

where $C_{\mathrm{d}1}$ is the drag coefficient in the along-cylinder direction and less dependent on the axial Reynolds number ($Re$) when $Re > 10^4$, but dependent on the cylinder's aspect ratio, $\delta = L/d$. An empirical formula is used for calculating $C_{\mathrm{d}1}$ [6],

$$C_{\mathrm{d}1} = \begin{cases} 1.0, & \text{if } \delta > 8, \\ 0.75 + \delta/32.1934 + 0.09612/\delta^2, & \text{if } 8 \geqslant \delta > 0.5, \\ 1.15, & \text{if } \delta \leqslant 0.5. \end{cases} \tag{12}$$

Substitution of (4) and (5) into (11) leads to

$$\mathbf{F}_{\mathrm{d}1} = -C_{\mathrm{td}1} I_{xx} \left( \begin{bmatrix} u \\ v \\ w \end{bmatrix} - \begin{bmatrix} u_{\mathrm{w}} \\ v_{\mathrm{w}} \\ w_{\mathrm{w}} \end{bmatrix} \right), \quad I_{xx} = \mathbf{i}_{\mathrm{F}} \mathbf{i}_{\mathrm{F}}^{\mathrm{T}},$$

where the superscript 'T' denotes the transpose, and $C_{\mathrm{td}1}$ is the drag coefficient along the cylinder (in the $\mathbf{i}_F$ direction) for the relative motion between COM and water (or called the translational drag).

The drag force along-$\mathbf{j}_F$ is calculated by

$$\begin{aligned} \mathbf{F}_{\mathrm{d}2} &= \left[ d \int_{-\frac{L}{2}-\chi}^{\frac{L}{2}-\chi} \frac{1}{2} C_{\mathrm{d}2} (V_2')^2 \frac{\rho_{\mathrm{w}}}{(1+f_2)} \mathrm{d}\eta \right] \mathbf{j}_{\mathrm{F}} \\ &= (C_{\mathrm{td}2} V_2 + f_{\mathrm{rd}2}) \mathbf{j}_{\mathrm{F}}, \end{aligned} \tag{13}$$

where

$$V_2'(\eta) = V_2 - \omega_3' \eta,$$

is the water-to-cylinder velocity at the surface in the $\mathbf{j}_F$ direction and

$$C_{\mathrm{td}2} \equiv C_{\mathrm{d}2} L d \frac{\rho_{\mathrm{w}}}{(1+f_2)} \left( \frac{V_2}{2} + \chi \omega_3' \right), \tag{14a}$$

is the translational drag coefficient and

$$f_{\mathrm{rd}2} \equiv C_{\mathrm{d}2} L d \frac{\rho_{\mathrm{w}}}{(1+f_2)} \left( \frac{1}{2}\chi^2 + \frac{1}{24} L^2 \right) \omega_3'^2, \tag{14b}$$

is the rotational drag force in the $\mathbf{j}_F$ direction. Here, $C_{\mathrm{d}2}$ is the drag coefficient for the across-cylinder direction. An empirical formula is used for calculating $C_{\mathrm{d}2}$ [7,6]

$$C_{\mathrm{d}2} = \begin{cases} 1.9276 + 8/Re, \\ \quad \text{if } Re \leqslant 12 \\ 1.261 + 16/Re, \\ \quad \text{if } 12 < Re \leqslant 180 \\ 0.855 + 89/Re, \\ \quad \text{if } 180 < Re \leqslant 2000 \\ 0.84 + 0.00003Re, \\ \quad \text{if } 2000 < Re \leqslant 12,000 \\ 1.2 - 4/\delta \\ \quad \text{if } 12,000 < Re \leqslant 150000, \delta \geqslant 10 \\ 0.835 - 0.35/\delta, \\ \quad \text{if } 12,000 < Re \leqslant 150,000, 2 \leqslant \delta < 10 \\ 0.7 - 0.08/\delta, \\ \quad \text{if } 12,000 < Re \leqslant 150,000, \delta < 2 \\ 1.875 - 0.0000045Re, \\ \quad \text{if } 150,000 < Re \leqslant 350,000 \\ 1/(641550/Re + 1.5), \\ \quad \text{if} Re > 350,000. \end{cases} \tag{15}$$

Substitution of (4) and (5) into (13) leads to

$$\mathbf{F}_{\mathrm{d}2} = -C_{\mathrm{td}2} I_{yy} \left( \begin{bmatrix} u \\ v \\ w \end{bmatrix} - \begin{bmatrix} u_{\mathrm{w}} \\ v_{\mathrm{w}} \\ w_{\mathrm{w}} \end{bmatrix} \right) + f_{\mathrm{rd}2} \mathbf{j}_{\mathrm{F}}, \quad I_{yy} = \mathbf{j}_{\mathrm{F}} \mathbf{j}_{\mathrm{F}}^{\mathrm{T}}. \tag{16}$$

The angular velocity ($\omega_2'$) around $\mathbf{j}_F$ causes non-uniform water-to-cylinder velocity in the $\mathbf{k}_F$ direction

$$V_3 = \omega_2' \eta. \tag{17}$$

The drag force along-$\mathbf{k}_F$ is calculated by

$$\begin{aligned} \mathbf{F}_{\mathrm{d}3} = &\left[ \frac{1}{2} C_{\mathrm{d}2} d \frac{\rho_{\mathrm{w}}}{(1+f_2)} \omega_2' |\omega_2'| \left( \int_0^{\frac{L}{2}-\chi} \eta^2 \mathrm{d}\eta \right.\right. \\ &\left.\left. - \int_{-\frac{L}{2}-\chi}^{0} \eta^2 \mathrm{d}\eta \right) \right] \mathbf{k}_{\mathrm{F}} = f_{\mathrm{rd}3} \mathbf{k}_{\mathrm{F}}, \end{aligned} \tag{18}$$

where

$$f_{\mathrm{rd}3} \equiv -\frac{1}{12} C_{\mathrm{d}2} \frac{\rho_{\mathrm{w}} d}{(1+f_2)} \chi (3L^2 + 4\chi^2) |\omega_2'| \omega_2', \tag{19}$$

is the rotational drag force in the $\mathbf{k}_F$ direction.

### *4.2. Lift force*

The water-to-cylinder velocity determines the lift force [1]

$$\mathbf{F}_{\mathrm{l}} = \left[\frac{C_{\mathrm{tl}}}{L}\int_{-\frac{L}{2}-\chi}^{\frac{L}{2}-\chi} V_2'(\eta)d\eta\right]\mathbf{k}_{\mathrm{F}}, \quad C_{\mathrm{tl}} \equiv \frac{1}{2}C_{\mathrm{l}}Ld \times \frac{\rho_{\mathrm{w}}}{(1+f_2)}\mid V_2\mid, \tag{20}$$

where $C_{\mathrm{l}}$ is the lift coefficient. An empirical formula is used for calculating $C_{\mathrm{l}}$ [8],

$$C_{\mathrm{l}} = \begin{cases} \omega_1 d/V_2, & \text{if } \omega_1 d/V_2 \leqslant 8, \\ 8 + 0.12(\omega_1 d/V_2 - 8), & \text{if } \omega_1 d/V_2 > 8 \end{cases} \tag{21}$$

and $C_{\mathrm{tl}}$ is the translational lift coefficient. Substitution of (4), (5), (14) into (20) leads to

$$\mathbf{F}_{\mathrm{l}} = -C_{\mathrm{tl}}I_{yz}\left(\begin{bmatrix} u \\ v \\ w \end{bmatrix} - \begin{bmatrix} u_{\mathrm{w}} \\ v_{\mathrm{w}} \\ w_{\mathrm{w}} \end{bmatrix}\right) + f_{\mathrm{rl}}\mathbf{k}_{\mathrm{F}}, \quad I_{yz} = \mathbf{k}_{\mathrm{F}}\mathbf{j}_{\mathrm{F}}^{\mathrm{T}}, \tag{22}$$

where

$$f_{\mathrm{rl}} \equiv C_{\mathrm{tl}}\chi\omega_3',$$

is the rotational lift force.

### 4.3. Hydrodynamic torque

For an axially symmetric cylinder, the hydrodynamic torque in the $\mathbf{i}_F$ direction is not caused by the drag and lift forces, but by the viscous fluid. The moment of the viscous force of steady flow between two rotating cylinders with the common axis is calculated by [5]

$$M = 4\pi\mu\frac{r_1^2 \cdot r_0^2}{r_1^2 - r_0^2}(\omega_1 - \omega_0), \tag{23}$$

where $(r_1, r_0)$ and $(\omega_1, \omega_0)$ are the radii and angle velocities of the inner and outer cylinders; $\mu$ is the viscosity. Moment of the viscous force on one rotating cylinder is the limit case of the two rotating cylinders as $r_0 \to \infty$, $\omega_0 = 0$. The moment of the viscous force around $\mathbf{i}_F$ is calculated by

$$\mathbf{M}_{\mathrm{d1}} = -C_{m1}\omega_1\mathbf{i}_{\mathrm{F}}, C_{m1} \equiv \pi\mu Ld^2. \tag{24}$$

When the cylinder rotates around $\mathbf{j}_F$ with the angular velocity $\omega_2'$, the drag force causes a torque on the cylinder in the $\mathbf{j}_{\mathrm{F}}$ direction

$$\mathbf{M}_{\mathrm{d2}} = \left[-\omega_2'|\omega_2'|\int_{-\frac{L}{2}-\chi}^{\frac{L}{2}-\chi}\frac{1}{2}C_{\mathrm{d2}}d\frac{\rho_{\mathrm{w}}}{(1+f_{\mathrm{r}})}\eta^2|\eta|\mathrm{d}\eta\right]\mathbf{j}_{\mathrm{F}} = -\left[C_{m2}\omega_2'\right]\mathbf{j}_{\mathrm{F}}, \tag{25}$$

$$C_{m2} \equiv \frac{1}{4}C_{\mathrm{d2}}d\frac{\rho_{\mathrm{w}}}{(1+f_{\mathrm{r}})}\left(\frac{1}{16}L^4 + \frac{3}{2}L^2\chi^2 + \chi^4\right)|\omega_2'|, \tag{26}$$

where $f_{\mathrm{r}}$ is the added mass factor for the moment of drag and lift forces. If the water-to-cylinder velocity or the cylinder mass distribution is non-uniform ($\chi \neq 0$), the drag force causes a torque on the cylinder in the $\mathbf{k}_F$ direction

$$\mathbf{M}_{\mathrm{d3}} = \left[\int_{-\frac{L}{2}-\chi}^{\frac{L}{2}-\chi}\frac{1}{2}C_{\mathrm{d2}}d\frac{\rho_{\mathrm{w}}}{(1+f_{\mathrm{r}})}\left(V_2 - \omega_3'\eta\right)^2\eta\mathrm{d}\eta\right]\mathbf{k}_F = -\left[C_{m3}\omega_3' + M_3\right]\mathbf{k}_F, \tag{27}$$

$$C_{m3} \equiv C_{\mathrm{d2}}d\frac{\rho_{\mathrm{w}}}{(1+f_{\mathrm{r}})} \times \left(\frac{1}{12}V_2L^3 + V_2L\chi^2 + \frac{1}{8}L^3\omega_3'\chi + \frac{L}{2}\chi^3\omega_3'\right), \tag{28}$$

$$M_3 \equiv \frac{1}{2}C_{\mathrm{d2}}d\frac{\rho_{\mathrm{w}}}{(1+f_{\mathrm{r}})}V_2^2L\chi. \tag{29}$$

The lift force exerts a torque on the cylinder in the $\mathbf{j}_F$ direction

$$\mathbf{M}_{\mathrm{l2}} = \left[-\int_{-\frac{L}{2}-\chi}^{\frac{L}{2}-\chi}\frac{1}{2}C_{\mathrm{l}}d\frac{\rho_{\mathrm{w}}}{(1+f_{\mathrm{r}})}\left(V_2 - \omega_3'\eta\right)\eta\mathrm{d}\eta\right]\mathbf{j}_{\mathrm{F}} = \left[C_{m\mathrm{l}}\omega_3' + M_1\right]\mathbf{j}_{\mathrm{F}}, \tag{30}$$

$$C_{m\mathrm{l}} \equiv C_{\mathrm{l}}V_2d\frac{\rho_{\mathrm{w}}}{(1+f_{\mathrm{r}})}L\left(\frac{1}{24}L^2 + \frac{\chi^2}{2}\right), \quad M_1 \equiv \frac{1}{2}\frac{\rho_{\mathrm{w}}}{(1+f_{\mathrm{r}})}LV_2^2\chi. \tag{31}$$

## 5. Composition of model cylinders

### 5.1. Description

Three model cylinders were used for the drop experiment at the Naval Postgraduate School swimming pool. All have the same diameter of 0.04 m, but different lengths of 0.152, 0.121 and 0.091 m. The bodies are constructed of rigid plastic with aluminum-capped ends. Inside each was a threaded bolt, running lengthwise across the cylinder, and an internal mass (Fig. 3). The internal cylindrical mass made of copper is used to vary the cylinder's center of mass and could be adjusted fore or aft.

The model cylinder is composed of six uniform cylindrical parts (Fig. 4): (1) a plastic hollow cylinder, (2) an aluminum-capped left end solid cylinder, (3) an aluminum-capped right end solid cylinder, (4) a cylindrical threaded rod, (5) a cylindrical threaded bolt, and (6) an adjustable copper cylindrical mass with the distance ($\lambda$) between its COMP and the geometric center of the model cylinder (**B**). The mass in each cylindrical part is uniformly distributed. Therefore, the center of mass for the part (COMP) is located at its center of volume. The geometric characteristics such as radius (or outer and inner radii), length, COMP location are listed in Tables 1 and 2. The density of each part is listed in Table 3.

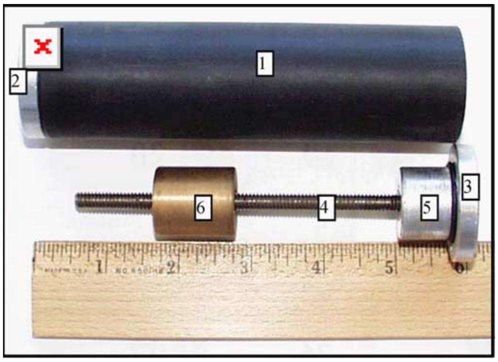


Fig. 3. Internal components of the model cylinder: (1) an plastic hollow cylinder; (2) an aluminum-capped left end solid cylinder; (3) an aluminum-capped right end solid cylinder, (4) a cylindrical threaded rod; (5) a cylindrical threaded bolt, and (6) an adjustable copper cylindrical mass.

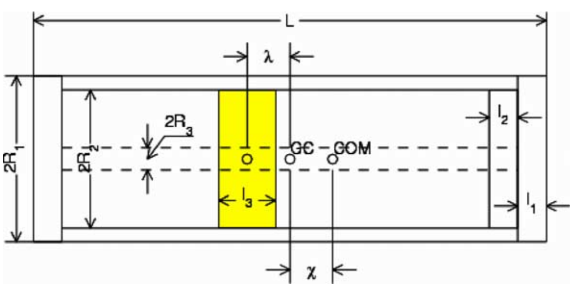


Fig. 4. Internal structure of the model cylinder.

Table 1
Characteristics of cylindrical parts

| Cylindrical parts | Mass | Radius/outer and inner radii | Length | Location of COMP in the $M$-coordinate |
|---|---|---|---|---|
| 1 | $m_1$ | $(R_1, R_2)$ | $L-2l_1$ | $\chi$ |
| 2 | $m_2$ | $R_1$ | $l_1$ | $L/2-l_1/2+\chi$ |
| 3 | $m_3$ | $R_1$ | $l_1$ | $L/2-l_1/2-\chi$ |
| 4 | $m_4$ | $R_3$ | $L-2l_1$ | $\chi$ |
| 5 | $m_5$ | $(R_2, R_3)$ | $l_2$ | $L/2-l_1-l_2/2-\chi$ |
| 6 | $m_6$ | $(R_2, R_3)$ | $l_3$ | $\lambda+\chi$ |

Table 2
Geometric parameters of the cylindrical parts (unit: $10^{-2}$ m)

| Cylinder | $R_1$ | $R_2$ | $R_3$ | $l_1$ | $l_2$ | $l_3$ | $L$ |
|---|---|---|---|---|---|---|---|
| 1 | 2.0 | 1.2 | 0.3 | 0.6 | 1.9 | 2.7 | 15.2 |
| 2 | 2.0 | 1.2 | 0.3 | 0.6 | 1.9 | 2.7 | 12.1 |
| 3 | 2.0 | 1.2 | 0.3 | 0.6 | 1.9 | 2.7 | 9.1 |

Table 3
Density (unit: $10^3$ kg m$^{-3}$) of the materials for the model cylinder

| Material | Aluminum | Copper | Plastic | Steel |
|---|---|---|---|---|
| Density | 2.70 | 8.93 | 1.16 | 7.80 |

Table 4
Moments of gyration of the six cylindrical parts

| Cylindrical part | $J_1$ | $J_2 = J_3$ |
|---|---|---|
| 1 | $\frac{m_1}{2}(R_1^2+R_2^2)$ | $\frac{m_1}{12}\left[3R_1^2+3R_2^2+(L-2l_1)^2\right]$ |
| 2 | $\frac{m_2}{2}R_1^2$ | $\frac{m_2}{12}(3R_1^2+l_1^2)$ |
| 3 | $\frac{m_3}{2}R_1^2$ | $\frac{m_3}{12}(3R_1^2+l_1^2)$ |
| 4 | $\frac{m_4}{2}R_3^2$ | $\frac{m_4}{12}\left[3R_3^2+(L-2l_1)^2\right]$ |
| 5 | $\frac{m_5}{2}R_3^2$ | $\frac{m_5}{12}(3R_2^2+3R_3^2+l_2^2)$ |
| 6 | $\frac{m_6}{2}(R_2^2+R_3^2)$ | $\frac{m_6}{12}(3R_2^2+3R_3^2+l_3^2)$ |

### 5.2. Moments of gyration

The moments of gyration are defined by von Mises [1]

$$J_1=\int(y^2+z^2)\mathrm{d}m,\quad J_2=\int(z^2+x^2)\mathrm{d}m,$$
$$J_3=\int(x^2+y^2)\mathrm{d}m, \tag{32}$$

where $(x,y,z)$ are coordinates in the $M$-coordinate system. Since the six parts of the cylinders (or hollow cylinders) have uniform mass distribution, the moments of gyration for the part (i) are easily calculated (Table 4). The resultant moments of gyration ($J_1$, $J_2$, $J_3$) for the cylinder are computed by

$$J_1=\sum_{i=1}^{6}J_1^{(i)},$$
$$J_2=J_3=\sum_{i=1}^{6}J_2^{(i)}+m_1\chi^2+m_2\left(\frac{L-l_1}{2}-\chi\right)^2$$
$$+m_3\left(\frac{L-l_1}{2}+\chi\right)^2+m_4\chi^2+m_5\left(\frac{L}{2}-\chi-l_1\frac{l_2}{2}\right)^2$$
$$+m_6(\lambda+\chi)^2. \tag{33}$$

The location of COM ($\chi$) is determined by

$$\chi=\frac{[m_5(L/2-l_1-l_2/2)-m_6\lambda]}{\sum_{j=1}^{6}m_j}, \tag{34}$$

which indicates how the adjustable weight determines the location of COM for the model cylinder.

## 6. Similarity for experimental design

Most Russian sea mines usually have cylindrical geometry. Small and large aircraft-laid mines AMD-1 -500 and AMD-1-1000, were developed in 1942. Later, they are ranked high among their best foreign counterparts. At the end of WWII (in 1945), the upgraded versions of these mines appeared. They were designated AMD-2-500 and AMD-2-1000, respectively. These mines are designed to destroy surface warships and other vessels, as well as submarines. Weight and size of the small mine are similar to those of the FAB-500 aerial bomb (500 kg, $d \sim 0.45$ m), and of the large mine (1500 kg, $d \sim 0.533$ m) to those of the FAB-1500 aerial bomb. Standard aircraft attachment points were used to suspend the mines. Bottom mines (except for the AMD-1-500) can be scattered from surface ships and motor torpedo boats, while the two classes of the large mines can be deployed from the above platforms and from submarines. The aspect ratio ($L/d$) is always much smaller than 10 [9].

### 6.1. Geometric similarity

Consider the shallow water scenario of naval operation with water depths of 12.19–60.96 m (i.e., 40–200 ft) [10]. Our goal was to choose a scale that was somewhat representative of the real world ratio of water depth to mine length, but at the same time would be large enough to film and would not damage the pool's bottom. The model cylinders were based on the realistic assumption that a full mine with length of 3 m is laid in water depths of 45 m, thus producing a 15:1 ratio. The depth of the pool is 2.4 m. From this ratio, the length ($L$) of the model mine is chosen as 0.152 m. The addition of a 0.121 and 0.091 m length allowed for later comparison of the sensitivity of water phase trajectory to the ratio of mine length over diameter. The outer radius of the model mine is 0.02 m. The aspect (length/diameter) ratios ($L/d$) are 3.8, 3.025, and 2.28.

### 6.2. Similarity of buoyancy effect

Usually, the density ratio ($\rho/\rho_w$) of a full size mine is 1.8. The model cylinders with lengths of 0.152, 0.121, 0.091 m have densities of $(1.69, 1.67, 1.88) \times 10^3\,\mathrm{kg\,m^{-3}}$, and the corresponding density ratios of (1.70, 1.68, 1.88). In each of the three model cylinders, the location of the weight (i.e., the value of $\lambda$) is adjustable. Use of (34) location of the COM ($\chi$-value) can be determined (Table 5). The positive $\chi$-value indicates that COM is below COV, and the negative $\chi$-value indicates that COM is above COV. The maximum ratio of $\chi/L$ is about 0.10, 0.08, and 0.06 for the three model cylinders. Thus, the buoyancy force and torque are similar between the model cylinders and the full size mines.

### 6.3. Hydrodynamic similarity

Hydrodynamic force and torque depend on the drag coefficients ($C_{d1}$, $C_{d2}$) and lift coefficient $C_l$. The drag coefficients (12) and (15) depends on the aspect ratio $\delta$ and axial Reynolds number ($Re$)

$$Re = \frac{Vd}{\nu}, \tag{35}$$

where $\nu = 0.18 \times 10^{-5}\ \mathrm{m^2\,s^{-1}}$, is molecular viscosity of the water. The diameter of the model cylinder ($d = 0.04$ m) is around 1/10 of the full size mine. Usually, the model cylinders (or full size mines) accelerate after entering the water surface. The axial Reynolds number increases with time. For the shallow water scenario, a full size mine may have a maximum speed just few times larger than that of the model cylinder. For $V \sim 2\,\mathrm{m\,s^{-1}}$, the axial Reynolds number is $0.44 \times 10^5$ for the model cylinders and $0.44 \times 10^6$ for the full size mine. Since it is likely $Re > 10^4$ for the model cylinder (or the full size mine) falling through the water column, the drag coefficient along the cylinder ($C_{d1}$) depends only on the aspect ratio $\delta$ [see (12)], and therefore is comparable for the model cylinder and for the full size mine due to similar aspect ratios.

The drag coefficient across the cylinder ($C_{d2}$) has a more complicated relationship than $C_{d1}$ [see (15)]. Although the maximum axial Reynolds number is at least 10 time larger for the full mines than for the model cylinders, it is possible the axial Reynolds numbers for the full size mine and model cylinder fall into the same interval as indicated in (15) in descending through the water column. The phenomenon observed for the model cylinders may be extrapolated into the full size mines with careful consideration of the range of the axial Reynolds number.

## 7. Cylinder drop experiment

A cylinder drop experiment was conducted at the NPS swim pool in June 2001. The purpose of the experiment is to collect data about cylinder's motion in the water column for various combinations of the model

Table 5
Physical parameters of the model cylinders

| Cylinder | Mass (kg) | $L$ (m) | Volume ($10^{-6}\,\mathrm{m^3}$) | $\rho_m$ ($10^3\,\mathrm{kg\,m^{-3}}$) | $J_1$ ($10^{-4}\,\mathrm{kg\,m^2}$) | $\chi$ ($10^{-2}$ m) | $J_2$ ($J_3$) ($10^{-4}\,\mathrm{kg\,m^2}$) |
|---|---|---|---|---|---|---|---|
| 1 | 0.3225 | 0.152 | 191.01 | 1.69 | 0.3305 | 0.00 | 6.0879 |
| | | | | | | 0.74 | 5.7830 |
| | | | | | | 1.48 | 6.2338 |
| 2 | 0.2542 | 0.121 | 152.05 | 1.67 | 0.2713 | 0.06 | 3.4246 |
| | | | | | | 0.53 | 3.2065 |
| | | | | | | 1.00 | 3.3126 |
| 3 | 0.2153 | 0.0912 | 114.61 | 1.88 | 0.2350 | 0.00 | 1.6952 |
| | | | | | | 0.29 | 1.5775 |
| | | | | | | 0.58 | 1.5568 |

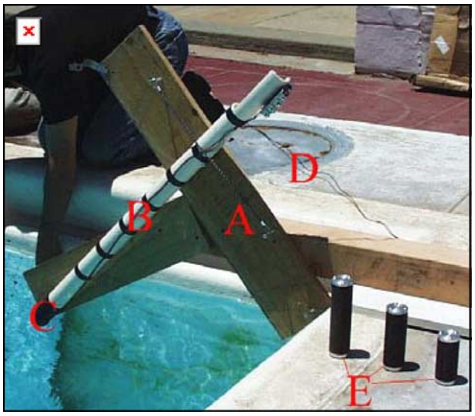


Fig. 5. Experimental equipments: (A) drop angle device, (B) cylinder injector, (C) infrared light sensor, (D) output to universal counter, and (E) cylinders.

mine parameters. The purpose is to detect the characteristics of the cylinder's movement in the water column and to collect the data of the location, orientation.

It basically consisted of dropping each of three model cylinders into the water where each drop was recorded underwater from two viewpoints. Fig. 5 depicts the overall setup. The controlled parameters for each drop were: $L/d$ ratio, $\chi$-value, initial speed ($V^{(\mathrm{in})}$), and drop angle. The $E$-coordinate system is chosen with the origin at the corner of the swimming pool with the two sides as $x$- and $y$-axis and the vertical $z$-axis. The initial injection of cylinders was in the $(y, z)$ plane (Fig. 6).

### 7.1. Initial speed

Initial speed ($V^{(\mathrm{in})}$) was calculated by using the voltage return of an infrared photo detector located at the base of the cylinder injector. The infrared sensor produced a square wave pulse when no light was detected due to blockage caused by the cylinder's passage. The length of the square wave pulse was converted into time by using a universal counter. Dividing the cylinder's length by the universal counter's time yielded $V^{(\mathrm{in})}$. The cylinders were dropped from several positions within the injector mechanism in order to produce a range of $V^{(\mathrm{in})}$. The method used to determine $V^{(\mathrm{in})}$ required that the infrared light sensor be located above the water's surface. This distance was held fixed throughout the experiment at 10 cm.

### 7.2. Drop angle

The drop angle (initial value of $\psi_2^{(\mathrm{in})}$) was controlled using the drop angle device. Five screw positions marked the 15°, 30°, 45°, 60°, and 75°. The drop angles were determined from the lay of the pool walkway, which was assumed to be parallel to the water's surface. A range of drop angles was chosen to represent the various entry angles that air and surface laid mines exhibit in naval operation. This range produced velocities whose horizontal and vertical components varied in magnitude. This allowed for comparison of cylinder trajectory sensitivity with the varying velocity components.

### 7.3. Methodology

For each drop the cylinder was set to a $\chi$-value. For positive $\chi$-value, the cylinders were placed into the injector so that the COM was located below the geometric center. For negative $\chi$-value, the COM was located above the geometric center to release. A series of drops were then conducted in order of decreasing mine length for each angle. Table 6 indicates number of drops conducted for different drop angles and $\chi$-value for $L/d = 3.85$. Number of drops for other $L/d$ ratios $(3.025, 2.28)$ is comparable to that for $L/d$ ratio of 3.85. All together there were 230 drops. Each video camera had a film time of approximately one hour. At the

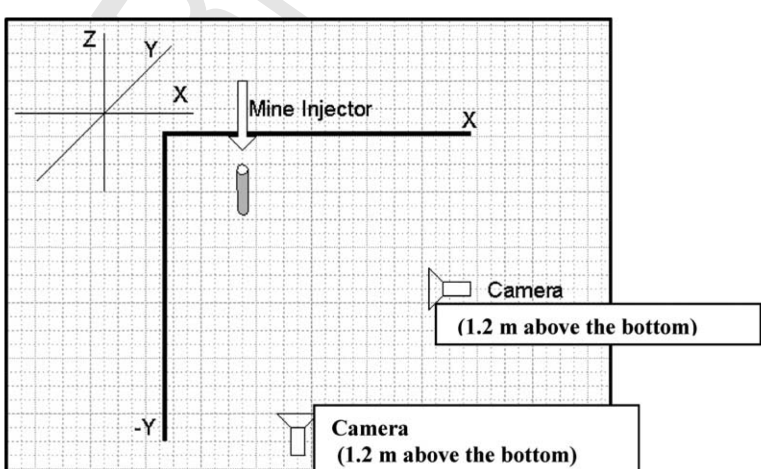


Fig. 6. Top view of the cylinder drop experiment. The two video cameras are in the middle of the water column (water depth 2.4 m).

Table 6
Number of drops conducted for different drop angles and $\chi$-values for $L/d = 3.85$

| $\psi_2^{(in)}$ | 15° | 30° | 45° | 60° | 75° |
|---|---|---|---|---|---|
| $\chi_2$ | 13 | 15 | 15 | 15 | 12 |
| $\chi_1$ | 9 | 15 | 15 | 15 | 9 |
| $\chi_0$ | 12 | 14 | 15 | 18 | 6 |
| $\chi_{-1}$ | 0 | 6 | 6 | 6 | 0 |
| $\chi_{-2}$ | 2 | 6 | 6 | 0 | 0 |

end of the day, the tapes were replayed in order to determine clarity and optimum camera position.

## 8. Data retrieval and analysis

### 8.1. Data retrieval

Upon completion of the drop phase, the video from each camera was converted to digital format. The digital video for each view was then analyzed frame by frame (30 Hz) in order to determine the mine's position in the $(x, z)$ and $(y, z)$ planes. The mine's top and bottom positions were input into a MATLAB generated grid, similar to the ones within the pool. The first point to impact the water was always plotted first. This facilitated tracking of the initial entry point throughout the water column. The cameras were not time synchronized; thus, the first recorded position corresponded to when the full length of the mine was in view.

### 8.2. Source of errors

There were several sources of error that hindered the determination of the cylinder's exact position within the water column. Locations above or below the camera's focal point were subjected to parallax distortion. Placing the cameras as far back as possible, while still being able to resolve the individual grid squares, minimized this error. Second, the background grids were located behind the cylinder's trajectory plane. This resulted in the cylinder appearing larger than normal. This error was minimized by neglecting that data if the plotted points exceed the particular cylinder's length. Third, an object injected into the water will generate an air cavity. This air cavity can greatly affect the initial motion, particularly at very high speeds (hydro ballistics). The air cavity effect was deemed to be minimal due to the low inject velocities used.

### 8.3. Data analysis

The data provided by each camera was first used to produce raw two 2-D plots of the cylinder's trajectory. Next, 2-D data from both cameras was then fused to produce a 3-D history. This 3-D history was then made non-dimensional in order to generalize the results. The non-dimensional data was used to generate impact scatter plots and was also used in multiple linear regression calculations.

## 9. Experimental results

### 9.1. Trajectory patterns

After analyzing the 3-D data set, seven trajectory patterns were found. The plots on the $(y, z)$ plane were chosen for trajectory analysis, as this plane was parallel to the direction of the mine drop. Observed trajectories (Fig. 7) were found to be most sensitive to $\chi$-value, drop angle and $L/d$ ratio (Table 7). Dependence of the trajectory patterns on the cylinders' physical parameters and release conditions are illustrated in Table 8 for $\chi > 0$ and Table 9 for $\chi < 0$.

For positive $\chi$-values (nose-down), as the distance between COM and COV increases (i.e., $\chi$ increases), the cylinder's trajectory tends to follow the straight pattern (Table 8). As the distance between COM and COV decreases (i.e., $\chi$ decreases), the cylinder's trajectory tends towards being more parallel with the pool's bottom. At steep drop angles, the cylinder experiences little lateral movement and tends towards a straight pattern. Additionally, as $L/d$ ratio decreased more complex trajectory patterns developed. This included significant oscillation about the vertical axis and increased lateral movement.

For negative $\chi$-values (nose-up), the cylinder will flip only once and almost all the flips occur right after entering the water surface. This is true for all 30 nose-up drop ($\chi < 0$) cases (Table 9). As the distance between COM and COV increases (i.e., $|\chi|$ increases), the cylinder's trajectory tends to follow the flip–straight pattern (Table 9). As the distance between COM and COV decreases (i.e., $\chi$ decreases), the cylinder's trajectory tends towards the flip–straight–spiral or flip–spiral pattern. Similar to the nose-down case, as $L/d$ ratio decreased more complex trajectory patterns developed.

### 9.2. Impact attitude

The angle, $\psi_2 + \pi/2$, is the impact attitude at the bottom of the water column. The mine burial is largely determined from the impact attitude of the cylinder. Cylinders whose impact attitudes are perpendicular ($\psi_2 = 90°$) to the sediment interface will experience the largest degree of impact burial [11]. It is therefore important to analyze the relationship between impact attitude and the controlled parameters, drop angle, $V^{(in)}$, $L/d$, and $\chi$. The experiment shows that both $L/d$ and $V^{(in)}$ had little influence on impact attitude. The impact atti-

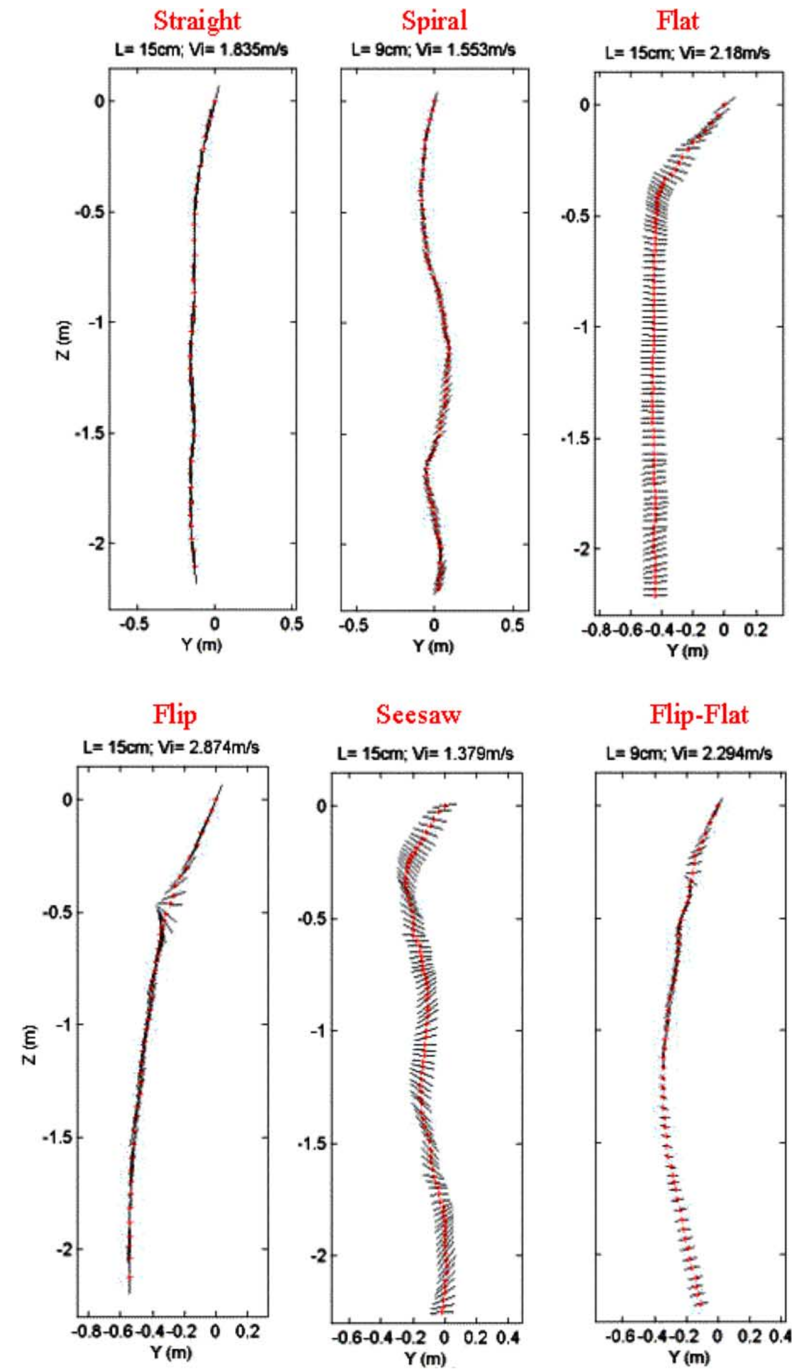


Fig. 7. Cylinders' track patterns observed during the experiment.

tude largely depends on the $\chi$-value. The histogram of the impact angle (Fig. 8) shows five peaks centered near 0°, 40°, 90°, 140°, and 180° corresponding to the COM positions $(\chi_{-2}, \chi_{-1}, \chi_0, \chi_1, \chi_2)$ [i.e., (COM-2, COM-1, COM0, COM1, COM2)].

Although drop angle is not the most influential parameter, variations did induce changes in impact orientation. As drop angle increases, the likelihood of any lateral movement decreases. This allowed for impact angles that are more vertically orientated. This is primarily due to the fact that the vertical components of velocity are greater than those at shallow angles. Thus, the time to bottom and time for trajectory alteration is less.

## 10. Numerical simulation

A numerical model on the base of momentum balance (7) and moment of momentum balance (8) has been developed to predict the cylinder's translation velocity

Table 7
Characteristics of trajectory patterns

| Trajectory pattern | Description |
|---|---|
| Straight | Cylinder exhibited little angular change about $z$-axis. The attitude remained nearly parallel with $z$-axis (±15°). |
| Slant | Cylinder exhibited little angular change about $z$-axis. The attitude was 45° off $z$-axis (±15°). |
| Spiral | Cylinder experienced rotation about $z$-axis throughout the water column. |
| Flip | Initial water entry point rotated at least 180°. |
| Flat | Cylinder's angle with vertical near 90° for most of the trajectory. |
| Seesaw | Similar to the flat pattern except that cylinder's angle with vertical would oscillate between greater (less) than 90° and less (greater) than 90°—like a seesaw. |
| Combination | Complex trajectory where cylinder exhibited several of the above patterns. |

and orientation using the triple coordinate transform [3]. The numerical model predicts the motion of cylinder inside the water column reasonably well. Two examples are listed for illustration.

*Positive* $\chi$ *(nose-down)*. Cylinder #1 ($L = 0.152$ m, $\rho = 1.69 \times 10^3\,\mathrm{kg\,m^{-3}}$) with $\chi = 0.0074$ m is injected to the water with the drop angle 45°. The physical parameters of this cylinder are given by

$$m = 0.3225\,\mathrm{kg}, \quad J_1 = 0.3305 \times 10^{-4}\,\mathrm{kg\,m^2},$$
$$J_2 = J_3 = 5.783 \times 10^{-4}\,\mathrm{kg\,m^2}.$$

Undersea cameras measure the initial conditions

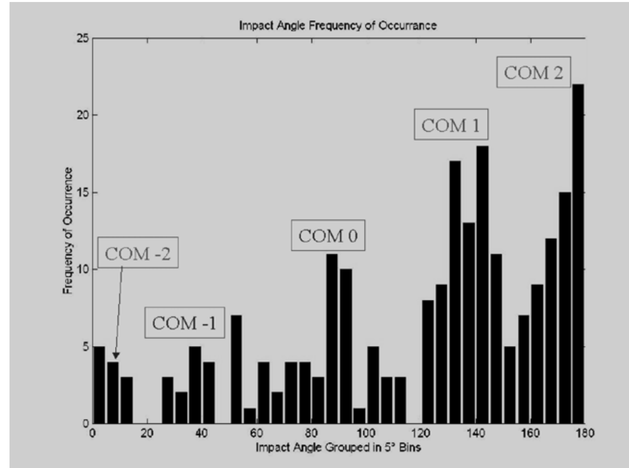


Fig. 8. Relationship between COM position and impact attitude.

$$\begin{aligned} &x_0 = 0, \quad y_0 = 0, \quad z_0 = 0, \quad u_0 = 0, \\ &v_0 = -1.55\,\mathrm{m\,s^{-1}}, \quad w_0 = -2.52\,\mathrm{m\,s^{-1}}, \\ &\psi_{10} = 0, \quad \psi_{20} = 60^\circ, \quad \psi_{30} = -95^\circ, \\ &\omega_{10} = 0, \quad \omega_{20} = 0.49\,\mathrm{s^{-1}}, \quad \omega_{30} = 0.29\,\mathrm{s^{-1}}. \end{aligned} \tag{36b}$$

Substitution of the model parameters (36a) and the initial conditions (36b) into the numerical model (see [3]) leads to the prediction of the cylinder's translation and orientation that are compared with the data collected during the experiment at time steps (Fig. 9). Both model simulated and observed tracks show a slant–straight pattern.

*Negative* $\boldsymbol{\chi}$ *(nose-up)*. Cylinder #2 ($L = 0.121$ m, $\rho = 1.67 \times 10^3\,\mathrm{kg\,m^{-3}}$) with $\chi = -0.01$ m is injected to the

Table 8
Dependence of trajectory patterns on input conditions for nose-down dropping ($\chi > 0$)

| | | | |
|---|---|---|---|
| Cylinder length (m) | 0.152 | 0.121 | 0.0912 |
| $\chi$ (m) | 0.0148 | 0.01 | 0.0058 |
| Drop angle 15° | Straight (1) slant–straight* (3) | Straight (1), spiral (1) slant–straight* (2) | Spiral* (2) straight–slant (1) slant–straight (1) |
| Drop angle 30° | Straight (1) slant–straight* (4) | Slant (1), spiral (1) straight (1) slant–straight* (2) | Spiral* (5) |
| Drop angle 45° | Slant* (2), straight (1) slant–straight (1) straight–spiral (1) | Straight (1) spiral* (2) straight–spiral (1) slant–straight (1) | Spiral* (4) slant–spiral (1) |
| Drop angle 60° | Straight** (5) | Straight* (3) Straight–spiral (1) straight–slant (1) | Spiral* (4) straight–spiral (1) |
| Drop angle 75° | Straight** (5) | Straight (2) straight–spiral (3) | Spiral (2), slant (1) straight–spiral (2) |

Here, the symbols '*' and '**' mean the dominant and only patterns in the given bin.

Table 9
Dependence of trajectory patterns on input conditions for nose-down dropping ($\chi < 0$)

| | | | |
|---|---|---|---|
| Cylinder length (m) | 0.1520 | 0.1210 | 0.0912 |
| $\chi$ (m) | 0.0 148 | 0.01 | 0.0058 |
| Drop angle 30° | Flip–straight* (3) flip–slant (1) | Flip–straight (2) flip–slant (2) | Flip–straight–spiral* (3) straight–flip–seesaw (1) |
| Drop angle 45° | Flip–straight* (2) Flip–slant (1) flip–spiral–slant (1) | Flip–straight (1) flip–slant* (2) flip–straight–spiral (1) | Flip–straight (1) flip–spiral* (2) flip–straight–spiral (1) |
| Drop angle 60° | Flip–straight (1) straight–flip (1) | Flip–straight (1) slant–flip–slant (1) | Flip–spiral–seesaw (1) flip–spiral (1) |

Here, the symbol '*' means the dominant pattern in the given bin.

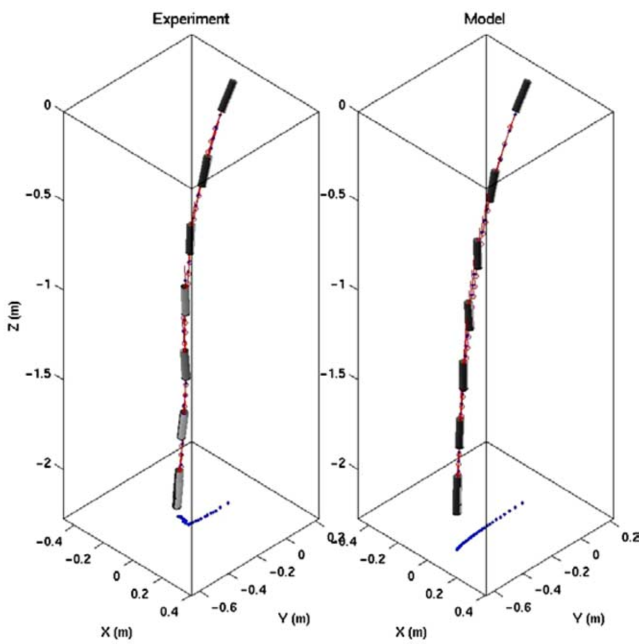


Fig. 9. Movement of cylinder #1 ($L = 0.152\,\text{m}$, $\rho = 1.69\times10^{3}\,\text{kg}\,\text{m}^{-3}$) with $\chi = 0.0074\,\text{m}$ and drop angle 45° obtained from: (a) experiment and (b) recursive model.

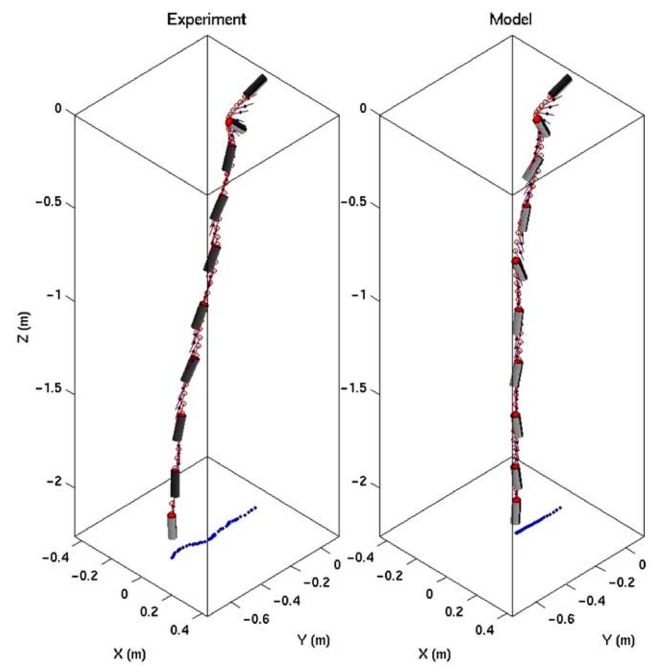


Fig. 10. Movement of cylinder #2 ($L = 0.121\,\text{m}$, $\rho = 1.67\times10^{3}\,\text{kg}\,\text{m}^{-3}$) with $\chi = -0.01\,\text{m}$ and drop angle 30° obtained from: (a) experiment and (b) recursive model.

water with the drop angle 30°. The physical parameters of this cylinder are given by

$$m = 0.2542\,\text{kg},\quad J_1 = 0.2713\times10^{-4}\,\text{kg}\,\text{m}^2,\quad J_2 = J_3 = 3.313\times10^{-4}\,\text{kg}\,\text{m}^2. \tag{37a}$$

Undersea cameras measure the initial conditions

$$\begin{aligned} &x_0 = 0,\quad y_0 = 0,\quad z_0 = 0,\quad u_0 = 0,\\ &v_0 = -0.75\,\text{m s}^{-1},\quad w_0 = -0.67\,\text{m s}^{-1},\\ &\psi_{10} = 0,\quad \psi_{20} = 24^\circ,\quad \psi_{30} = -96^\circ,\\ &\omega_{10} = 0,\quad \omega_{20} = -5.08\,\text{s}^{-1},\quad \omega_{30} = 0.15\,\text{s}^{-1}. \end{aligned} \tag{37b}$$

The predicted cylinder's translation and orientation are compared with the data collected during the experiment at time steps (Fig. 10). The simulated and observed tracks show a flip–spiral pattern. The flip occurs at 0.11 s (0.13 s) after the cylinder enters the water in the experiment (model). After the flip, the cylinder spirals down to the bottom.

## 11. Statistical analysis

Non-dimensional velocity data are got using

$$\mathbf{V} = \sqrt{gL}\,\mathbf{V}*. \tag{38}$$

Multivariate linear regression is conducted on the experimental data to establish relationships between the physical parameters of the cylinder ($L/d, \chi$), initial condition ($V^{*^{(in)}}, \psi_2^{(\text{in})}$) and the output data (temporally varying) such velocity ($u^*, v^*, w^*$) and attitude $\psi^{(2)}$ at time $t$. Let $Y(t)$ represent the output variables. The regression equation is given by

$$Y(t) = \beta_0(t) + \beta_1(t)\psi_2^{(\text{in})} + \beta_2(t)L/d + \beta_3(t)V^{*^{(\text{in})}} + \beta_4(t)\chi, \tag{39}$$

which is statistically significant on 0.01 confidence level after the correlation coefficient test. Fig. 11 shows the temporally varying regression coefficients for the variable $u^*$, $v^*$, $w^*$, and $\psi_2$. For the cylinder's attitude ($\psi_2$) the coefficient $\beta_4(t)$ is much larger than the other coefficients, which indicates that the cylinder's orientation (versus the vertical direction) is mainly determined by the location of COM (i.e., the value of $\chi$).

To show the dependence of impact of the cylinder at the bottom (i.e., horizontal location relative to the cylinder's surface entry point, orientation, velocity), the multivariate regression between the input non-dimensional parameters: $\psi_2^{(\text{in})}$, $L/d$, $V^{*(\text{in})}$, and $\chi$, and the final state (i.e., impact on the bottom) variables such as the horizontal position of COM ($x_m, y_m$), the velocity of COM ($u^*, v^*, w^*$) and the attitude $\psi_2$. Let $Z$ represent the output variables. The regression equation is given by

$$Z = \alpha_0 + \alpha_1\psi_2^{(\text{in})} + \alpha_2 L/d + \alpha_3 V^{*(in)} + \alpha_4\chi \tag{40}$$

with the regression coefficients ($\alpha_0, \alpha_1, \alpha_2, \alpha_3, \alpha_4$) for the output parameters given by Table 10. The impact altitude at the bottom is given by

$$\psi_2^{(\text{bot})} = 103 - 13.4\psi_2^{(\text{in})} - 0.501L/d + 1.045V^{*(\text{in})} + 472\chi,$$

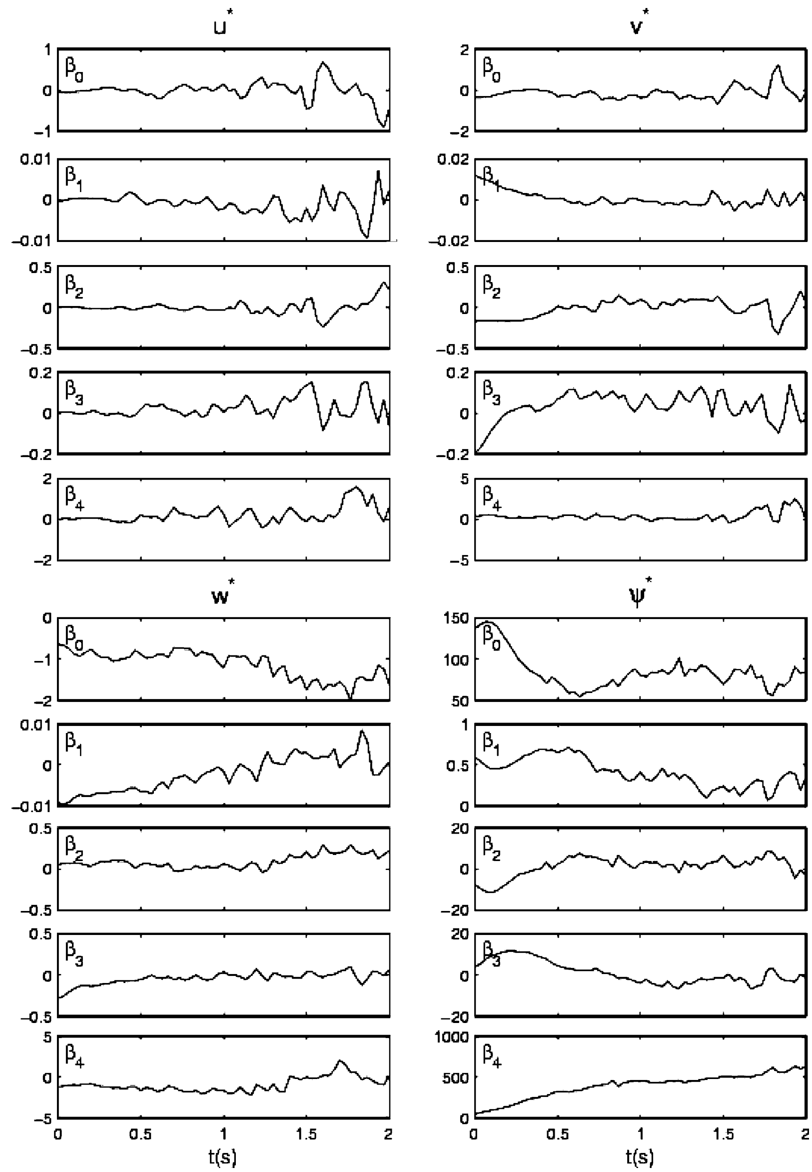


Fig. 11. Temporally varying regression coefficients.

Table 10
Regression coefficients of predicting bottom impact

| | | $\psi_2$ | u* | v* | w* |
|---|---|---|---|---|---|
| $\alpha_0$ | | 84.22 | −0.4675 | −0.1074 | −1.6268 |
| $\alpha_1$ | ($\psi_2^{(in)}$) | 0.354 | 0.002 | −0.0002 | 0.0006 |
| $\alpha_2$ | ($L/d$) | −3.329 | 0.216 | 0.0581 | 0.2251 |
| $\alpha_3$ | ($V^{*(in)}$) | −1.457 | −0.0063 | −0.0331 | 0.0615 |
| $\alpha_4$ | ($\chi$) | 625.65 | 0.591 | −0.0861 | 0.1657 |

where $\psi_2$ is in degree. The regression coefficients are 1–3 orders of magnitude smaller for ($L/d$) and $V^{*(in)}$ than for $\psi_2^{(in)}$ and $\chi$, which indicates that $L/d$ and initial water entry speed have little influence on cylinder's impact attitude on the bottom. For $\chi = 0$, the cylinder is almost parallel to the bottom. For $\chi_{-2}$ and $\chi_2$ cases (large $|\chi|$ value), the cylinder is almost vertical to the bottom.

## 12. Conclusions

(1) Movement of a falling cylinder in water column is a highly nonlinear process. Six trajectory patterns (straight, spiral, flip, flat, seesaw, combination) are detected from the experiment. The transition between patterns depends on the initial conditions (drop angle $\psi_2^{in}$) and initial speed $V^{(in)}$ and the physical parameters of the cylinder (such as $L/d$ ratio, $\chi$-value). All the nose-up drops ($\chi < 0$, 30 drops)

shows that the cylinder flips only once once for negative $\chi$-values. The flat pattern occurs usually for $\chi = 0$ (i.e., COM coincides with COV).

(2) The experiment shows that both $L/d$ and $V^{(in)}$ had little influence on cylinder's impact attitude on the bottom. The $\chi$-value is most important to determine the impact attitude. For $\chi = 0$, the cylinder is almost parallel to the bottom. For $\chi_{-2}$ and $\chi_2$ cases, the cylinder is almost vertical to the bottom.

(3) The experiment provides a data set of temporally varying cylinder's orientation, COM position and velocity for various input conditions such as cylinder's physical parameters and initial conditions. The data are useful for model development and validation.

(4) The cylinder's movement during the experiment is well simulated using a numerical model based on the momentum and moment of momentum balances with triple coordinate transform.

## Acknowledgement

This work was supported by the Office of Naval Research Marine Geology Program (N0001403WR20178) and the Naval Oceanographic Office (N6230603PO 30001).

## References

[1] R. Von Mises, Theory of Flight, first ed., Dover Publications Inc., New York, 1959, pp. 564–585.

[2] J.M. Boorda, Mine Countermeasures—An Integral Part of Our Strategy and Our Forces, Federation of American Scientists, Washington, DC, 1999, Available from: <http://www.fas.org/man/dod-101/sys/ship/weaps/docs/cnopaper.htm> .

[3] P.C. Chu, C.W. Fan, A.D. Evans, A. Gilles, Triple coordinate transforms for prediction of falling cylinder through the water column, Journal of Applied Mechanics 71 (2004) 292–298.

[4] S.F. Hoerner, Fluid-Dynamic Drag—Practical Information on Aerodynamic Drag and Hydrodynamic Resistence, 1st ed., Hoerner Fluid Dynamics, 1965, 259p.

[5] F.M. White, Viscous Fluid Flow, first ed., McGraw-Hill Inc., New York, 1974, p. 712.

[6] C.T. Crowe, J.A. Roberson, D.F. Elger, Engineering Fluid Mechanics, seventh ed., John Wiley & Sons Inc, New York, 2001, p. 714.

[7] H. Rouse, Fluid Mechanics for Hydraulic Engineers, first ed., Mcgraw-Hill Book Company Inc., New York, 1938, p. 422.

[8] B.M. Sumer, J. Fredsøe, Hydrodynamics Around Cylindrical Structures, first ed., World Scientific, Singapore, 1997, p. 530.

[9] S. Proshkin, Russian sea mines, Gidropribor Central Research Institute, Russia. Available from: <http://www.militarism.navy.ru/mines.htm> 1998.

[10] Ocean Study Board, Oceanography and Mine Warfare, National Academy Press, Washington DC, 2000. Available from: <http://www.nap.edu/books/0309067987/html/>.

[11] P.C. Chu, V.I. Taber, S.D. Haeger, A mine impact burial model sensitivity study. Institute of Joint Warfare Analysis, Naval Postgraduate School, Technical Report, NPS-IJWA-00-003, Monterey, CA, 2000, pp. 1–48.